Electronic Supplementary Information

Both end-on and end-to-end azide bridged tetranuclear ferromagnetic nickel(II) Schiff base complex

Anik Bhattacharyya[a], Mithun Das[a], Antonio Bauzá[b], Santiago Herrero[c], Rodrigo González-Prieto[c], Antonio Frontera[b,*] and Shouvik Chattopadhyay[a,*]

[a]Department of Chemistry, Inorganic Section, Jadavpur University, Kolkata - 700032, India.

Tel: +913324572941; E-mail: shouvik.chem@gmail.com

[b]Departamento de Química, Universitat de les Illes Balears, Crta. de Valldemossa km 7.5, 07122 Palma (Baleares), Spain.

[c] Departamento de Química Inorgánica, Facultad de Ciencias Químicas, Universidad Complutense de Madrid, Ciudad Universitaria, 28040 Madrid, Spain.

Experimental Section

Details of instrumentation

Elemental analysis (carbon, hydrogen and nitrogen) was performed using a PerkinElmer 240C elemental analyser. IR spectrum in KBr (4500-500 cm^{-1}) was recorded with a PerkinElmer Spectrum Two spectrophotometer. Electronic spectrum in DMSO was recorded on a PerkinElmer Lambda 35 UV-visible spectrophotometer. Steady state photoluminescence in DMSO was obtained in Shimadzu RF-5301PC spectrofluorometer at room temperature. Time dependent photoluminescence was recorded using Hamamatsu MCP photomultiplier (R3809) and was analysed by using IBHDAS6 software. The emission of the complex is tentatively attributed to the intra-ligand transitions modified by metal coordination. Intensity decay profile was fitted to the sum-of exponentials series

$$I(t) = \sum_i \alpha_i \exp\left(-t/\tau_i\right)$$

where a_i was a factor representing the fractional contribution to the time-resolved decay of the component with a lifetime of τ_i. Mono-exponential function was used to fit the decay profile for the complex, with obtaining χ^2 close to 1. The intensity-averaged life time (τ_{av}) was determined from the result of the exponential model using

$$\tau_{av} = \frac{\sum_i \alpha_i \tau_i^2}{\sum_i \alpha_i \tau_i}$$

where a_i and τ_i are the pre-exponential factors and excited-state luminescence decay time associated with the *i*-th component, respectively. Magnetic data were recorded using a SQUID magnetometer (Quantum Design MPMS-XL) over a temperature range of 1.8–300 K in a 0.2T external field. Corrections for diamagnetism were made using Pascal's constants and magnetic data were corrected for diamagnetic contributions from the sample holder. Powder X-ray diffraction was performed on a Bruker D8 instrument with Cu K_α radiation. In this process, the complexes were ground with a mortar and pestle to prepare fine powders. The powders were then dispersed with alcohol onto a zero background holder (ZBH). The alcohol was allowed to evaporate to provide a nice, even coating of powder adhered to the sample holder.

X-ray crystallography

A suitable crystal of the complex was picked, mounted on a glass fibre and diffraction intensities were measured with an Oxford Diffraction XCalibur, Eos equipped with Mo K_α radiation (λ = 0.71073 Å, 50 kV, 40 mA) at 150 K. CrysAlis^{PRO} program was used for data collection and processing.[S1] The intensities were corrected for absorption using the built in absorption correction method.[S2] The molecular structure was solved by direct method and refined by full-matrix least squares on F^2 using the WinGX[S3] software equipped with SHELXL-97.[S4] Non-hydrogen atoms were refined with anisotropic thermal parameters. Hydrogen atoms attached to oxygen atoms of methanol and water were located by difference Fourier maps and were kept at fixed positions. All other hydrogen atoms were placed in their geometrically idealized positions and constrained to ride on their parent atoms. CCDC reference number 971883.

Theoretical methods

The theoretical study is devoted to the rationalization of the magnetic results. The determination of J values was carried out using DFT[S5] calculations (B3LYP/6-31+G*)[S6] combined with the broken symmetry approach using GAUSSIAN-09 program.[S7] The magnetic coupling constants J of this system is described by the Heisenberg model, as described above. For the nickel(II) complex, the calculation of the J values (J_1 and J_2) has been performed computing the difference between the energy values of the highest spin (HS) state and the broken-symmetry (BS) state using the Yamaguchi[S8] formula, $J = (E_{BS} - E_{HS}) / (\langle S^2 \rangle_{HS} - \langle S^2 \rangle_{BS})$.

For the system studied herein DFT based wave functions have provided a reasonable estimate of exchange coupling constants. It should be mentioned that the widely and successfully used[S9] broken-symmetry DFT approach is not a unique methodology to compute and interpret the magnetic properties in quantum chemistry. For instance, *ab initio* methods based on difference dedicated configuration interaction[S10] (e.g., CASSCF/DDCI) give excellent results and offer the possibility to finely analyse the mechanisms and origin of the magnetic properties, taking advantage of access to the wave function of all spin states of interest. Moreover, for monometallic nickel(II) and cobalt(II) complexes with large magnetic anisotropy, it has been proposed a scheme to extract both the parameters of the zero-field splitting (ZFS) tensor and the magnetic anisotropy axes based on the effective Hamiltonian theory.[S11] Opposite to the typical theoretical procedure of extraction, this method determines the sign and the magnitude of the ZFS parameters in any circumstances. For instance, the energy levels provide enough information to extract the ZFS parameters in nickel(II) complexes, however additional information contained in the wave functions must be used to extract the ZFS parameters of cobalt(II) complexes.

The calculations of the noncovalent interactions were carried out using the TURBOMOLE[S12] version 7.0 using the BP86-D3/def2-TZVP level of theory. To evaluate the

interactions in the solid state, we have used the crystallographic coordinates. This procedure and level of theory have been successfully used to evaluate similar interactions.[S13] The interaction energies were computed by calculating the difference between the energies of isolated monomers and their assembly. The interaction energies were corrected for the Basis Set Superposition Error (BSSE) using the counterpoise method.[S14] Bader's "Atoms in molecules" theory has been used to study the interactions discussed herein by means of the AIMAll calculation package.[S15] The MEPS calculations have been performed by means of the SPARTAN software.[S16]

Results and Discussion

IR and electronic spectrum

In the IR spectrum (Fig. S5, ESI) of the complex distinct band due to the azomethine (C=N) group at 1631 cm^{-1} is routinely noticed.[S17] The strong band at 1091 cm^{-1} gives evidence for the presence of ionic perchlorate.[S18] Strong bands at 2054 and 2078 cm^{-1} in the IR spectrum of the complex indicates the presence of $\mu_{1,1}$ and $\mu_{1,3}$ azides respectively which are also evident from the crystal structure determination.[S19] A broad band around 3444 cm^{-1} is assigned to the O-H stretching vibration of the coordinated water molecule, which is involved in hydrogen bonding.[S20]

The electronic spectrum (Fig. S6, ESI) of the complex in DMSO displays absorption bands at 647 nm and 994 nm with a shoulder band at 893 nm. The first two bands are assigned to the spin allowed transitions $^3T_{1g}(F) \leftarrow {}^3A_{2g}(F)$ and $^3T_{2g}(F) \leftarrow {}^3A_{2g}(F)$ respectively, whereas the shoulder band is assigned as $^1E_g(D) \leftarrow {}^3A_{2g}(F)$.[S21] The higher energy d–d band, $^3T_{1g}(P) \leftarrow {}^3A_{2g}(F)$, is obscured by strong ligand to metal charge transfer transition ~380 nm, which is characteristic of nickel(II) complexes with Schiff base ligands.[S22] The band ~260 nm may be attributed to intra-ligand $\pi^* \leftarrow \pi$ transition of the Schiff base.[S23]

Photo-physical studies

The complex exhibits photoluminescence in DMSO medium at 424 nm on exciting at 380 nm. The mean lifetime (τ_{av}) of the exited state is 11.31 ns at room temperature. The lifetime decay profile of the complex is shown in Fig. S7, ESI.

X-ray powder diffraction pattern

The experimental PXRD pattern of the bulk product is in good agreement with the simulated XRD pattern from single crystal X-ray diffraction, indicating consistency of the bulk sample. The simulated pattern of the complex is calculated from the single crystal structural data (cif) using the CCDC Mercury software. Fig. S8 (ESI) shows the experimental and simulated powder XRD patterns of the complex.

References

S1 *CrysAlisPro*, Agilent Technologies, Version 1.171.35.21 (release 20-01-2012 CrysAlis171.NET), (compiled Jan 23 2012, 18:06:46).

S2 R. C. Clark and J. S. Reid, *Acta Cryst.*, 1995, **A51**, 887-897.

S3 L. J. Farrugia, *J. Appl. Cryst.*, 2012, **45**, 849-854.

S4 (a) G. M. Sheldrick, *Acta Cryst.*, 2015, **C71**, 3-8; (b) G. M. Sheldrick, *SHELXS - 97 and SHELXL - 97: Program for Structure Solution*, University of Gottingen, Institute fur Anorganische Chemieder Universitat, Gottingen, Germany, 1997.

S5 (a) L. Noodleman, *J. Chem. Phys.*, 1981, **74**, 5737; (b) L. Noodleman and D. A. Case, *Adv. Inorg. Chem.*, 1992, **38**, 423-458; (c) L. Noodleman, C. Y. Peng, D. A. Case and J. -M. Mouesca, *Coord. Chem. Rev.*, 1995, **144**, 199-244.

S6 (a) A. D. Becke, *J. Chem. Phys.*, 1993, **98**, 5648-5653; (b) C. Lee, W. Yang and R. G. Parr, *Phys. Rev. B: Condens. Matter*, 1988, **37**, 785-789.

S7 M. J. Frisch, G. W. Trucks, H. B. Schlegel, G. E. Scuseria, M. A. Robb, J. R. Cheeseman, G. Scalmani, V. Barone, B. Mennucci, G. A. Petersson, H. Nakatsuji, M. Caricato, X. Li, H. P. Hratchian, A. F. Izmaylov, J. Bloino, G. Zheng, J. L. Sonnenberg, M. Hada, M. Ehara, K. Toyota, R. Fukuda, J. Hasegawa, M. Ishida, T. Nakajima, Y. Honda, O. Kitao, H. Nakai, T. Vreven, J. A. Montgomery, J. J. E. Peralta, F. Ogliaro, M. Bearpark, J. J. Heyd, E. Brothers, K. N. Kudin, V. N. Staroverov, R. Kobayashi, J. Normand, K. Raghavachari, A. Rendell, J. C. Burant, S. S. Iyengar, J. Tomasi, M. Cossi, N. Rega, J. M. Millam, M. Klene, J. E. Knox, J. B. Cross, V. Bakken, C. Adamo, J. Jaramillo, R.

Gomperts, R. E. Stratmann, O. Yazyev, A. J. Austin, R. Cammi, C. Pomelli, J. W. Ochterski, R. L. Martin, K. Morokuma, V. G. Zakrzewski, G. A. Voth, P. Salvador, J. J. Dannenberg, S. Dapprich, A. D. Daniels, Ö. Farkas, J. B. Foresman, J. V. Ortiz, J. Cioslowski and D. J. Fox, *GAUSSIAN 09* (Revision C.01), Gaussian, Inc., Wallingford CT, 2009.

S8 (a) K. Yamaguchi, H. Fukui and T. Fueno, *Chem. Lett.*, 1986, 625-628; (b) M. Nishino, S. Yamanaka, Y. Yoshioka and K. Yamaguchi, *J. Phys. Chem. A*, 1997, **101**, 705-712.

S9 (a) N. Onofrio and J.-M. Mouesca, *Inorg. Chem.*, 2011, **50**, 5577–5586; (b) F. Neese, *Coord. Chem. Rev.*, 2009, **253**, 526–563; (c) F. Neese, T. Petrenko, D. Ganyushin and G. Olbrich, *Coord. Chem. Rev.*, 2007, **251**, 288–327; (d) C. Adamo, V. Barone, A. Bencini, R. Broer, M. Filatov, N. M. Harrison, F. Illas, J. P. Malrieu and I. de P. R. Moreira, *J. Chem. Phys.*, 2006, **124**, 107101; (e) C. Adamo and V. Barone, *J. Chem. Phys.*, 1999, **110**, 6158-6170; (f) C. Adamo, A. di Matteo and V. Barone, *Adv. Quantum Chem.*, 2000, **36**, 45-75.

S10 J. Miralles, O. Castell, R. Caballol and J. P. Malrieu, *Chem. Phys.*, 1993, **172**, 33-43.

S11 R. Maurice, R. Bastardis, C. de Graaf, N. Suaud, T. Mallah and N. Guihéry, *J. Chem. Theor. Comput.*, 2009, **5**, 2977-2984.

S12 R. Ahlrichs, M. Bär, M. Häser, H. Horn and C. Kölmel, *Chem. Phys. Lett.*, 1989, **162**, 165-169.

S13 (a) A. Bauzá, A. Terrón, M. Barceló-Oliver, A. García-Raso and A. Frontera, *Inorg. Chim. Acta.*, 2016, **452**, 244-250; (b) D. Sadhukhan, M. Maiti, G. Pilet, A. Bauzá, A. Frontera and S. Mitra, *Eur. J. Inorg. Chem.*, 2015, **11**, 1958-1972; (c) M. Mirzaei, H. Eshtiagh-Hosseini, Z. Bolouri, Z. Rahmati, A. Esmaeilzadeh, A. Hassanpoor, A. Bauza, P. Ballester, M. Barceló-Oliver, J. T Mague, B. Notash and A. Frontera, *Cryst. Growth Des.*, 2015, **15**, 1351–1361; (d) P. Chakraborty, S. Purkait, S. Mondal, A. Bauzá, A. Frontera, C. Massera and D. Das, *CrystEngComm*, 2015, **17**, 4680-4690.

S14 S. F. Boys and F. Bernardi, *Mol. Phys.*, 1970, **19**, 553-566.

S15 *AIMAll* (Version 13.05.06), A. Todd and T. K. Keith, Gristmill Software, Overland Park KS, USA, 2013.

S16 Y. Shao, L. F. Molnar, Y. Jung, J. Kussmann, C. Ochsenfeld, S. T. Brown, A. T. B. Gilbert, L. V. Slipchenko, S. V. Levchenko, D. P. O'Neill, R. A. DiStasio Jr., R. C. Lochan, T. Wang, G. J. O. Beran, N. A. Besley, J. M. Herbert, C. Y. Lin, T. Van Voorhis, S. H. Chien, A. Sodt, R. P. Steele, V. A. Rassolov, P. E. Maslen, P. P. Korambath, R. D. Adamson, B. Austin, J. Baker, E. F. C. Byrd, H. Dachsel, R. J. Doerksen, A. Dreuw, B. D. Dunietz, A. D. Dutoi, T. R. Furlani, S. R. Gwaltney, A. Heyden, S. Hirata, C.-P. Hsu, G. Kedziora, R. Z. Khalliulin, P. Klunzinger, A. M. Lee, M. S. Lee, W. Z. Liang, I. Lotan, N.

Nair, B. Peters, E. I. Proynov, P. A. Pieniazek, Y. M. Rhee, J. Ritchie, E. Rosta, C. D. Sherrill, A. C. Simmonett, J. E. Subotnik, H. L. Woodcock III, W. Zhang, A. T. Bell, A. K. Chakraborty, D. M. Chipman, F. J. Keil, A. Warshel, W. J. Hehre, H. F. Schaefer, J. Kong, A. I. Krylov, P. M. W. Gill and M. Head-Gordon, *Phys. Chem. Chem. Phys.,* 2006, **8**, 3172-3191.

S17. A. Bhattacharyya, P. K. Bhaumik, P. P. Jana and S. Chattopadhyay, *Polyhedron*, 2014, **78**, 40-45.

S18. A. Bhattacharyya, S. Sen, K. Harms and S. Chattopadhyay, *Polyhedron*, 2015, **88**, 156-163.

S19. S. S. Massoud, F. A. Mautner, R. Vicente, A. A. Gallo and E. Ducasse, *Eur. J. Inorg. Chem.*, 2007, 1091-1102.

S20. S. K. Ghosh and P. K. Bharadwaj, *Eur. J. Inorg. Chem.*, 2005, 4886-4889.

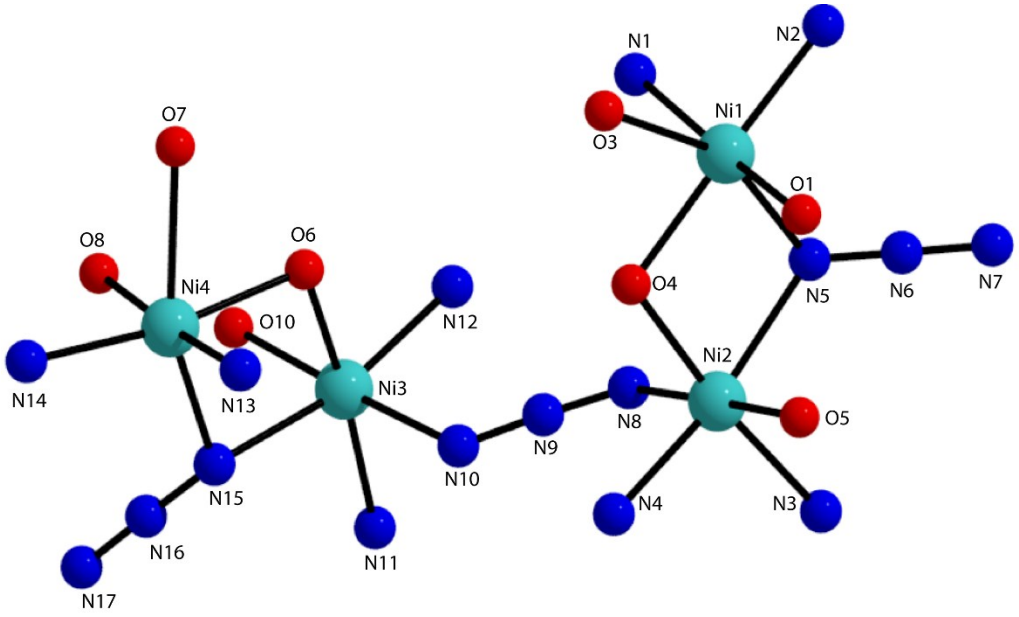

Fig. S1. Perspective view of the tetranuclear cationic unit with atom numbering scheme showing only coordinated atoms and bridging azides.

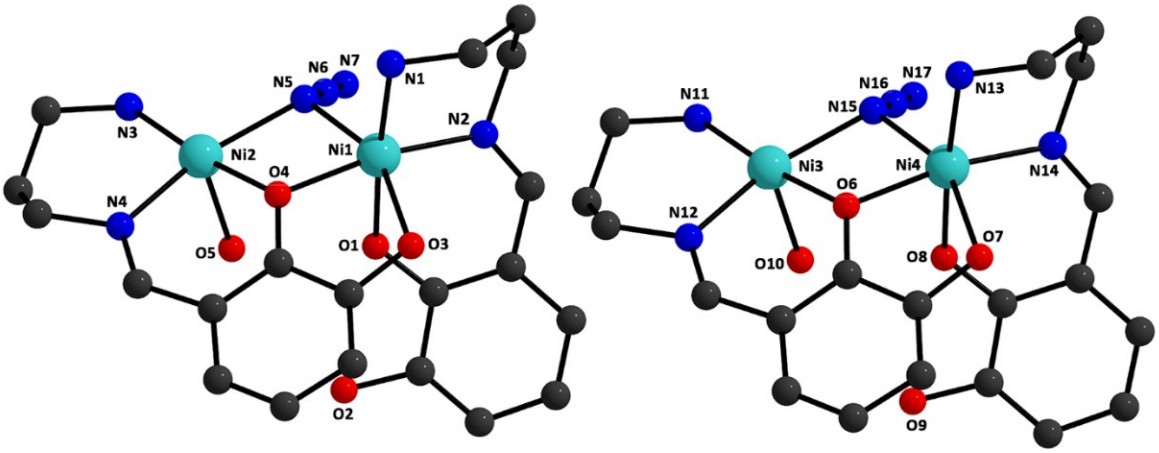

Fig. S2. Perspective views of two pseudo dinuclear units of the complex with selective atom numbering scheme. Hydrogen atoms and methyl groups have been omitted for clarity.

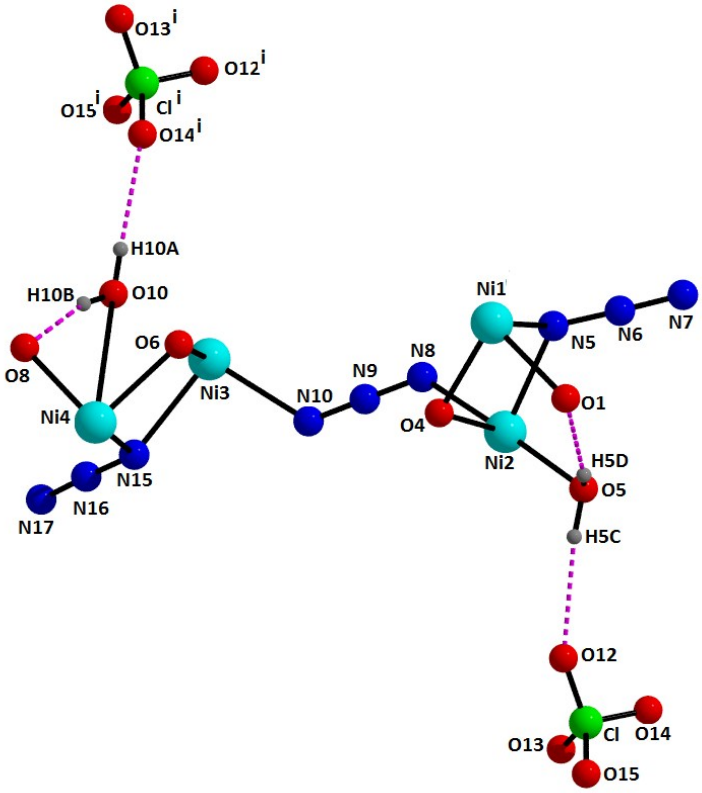

Fig. S3. Perspective view of hydrogen bonding interactions of the complex with atom numbering scheme. Only relevant atoms are shown. Symmetry transformation: ^{i} = -1+x,y,-1+z.

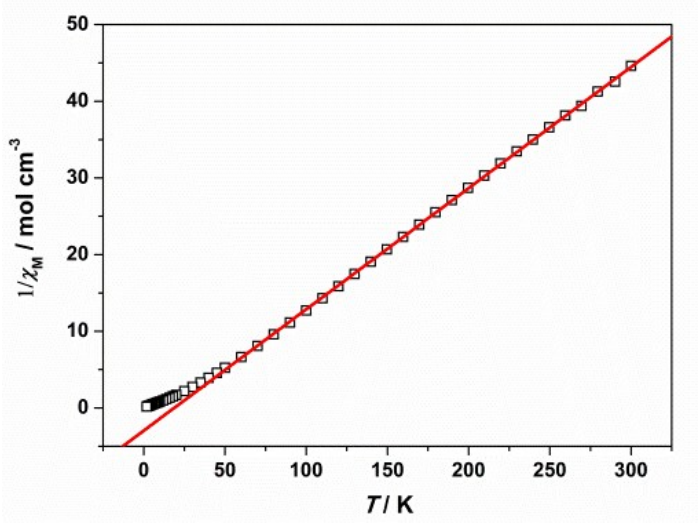

Fig. S4. Reciprocal susceptibility (□) *versus* temperature for the complex. The solid red line indicates the best fit to the Curie-Weiss law in the range 50-300 K.

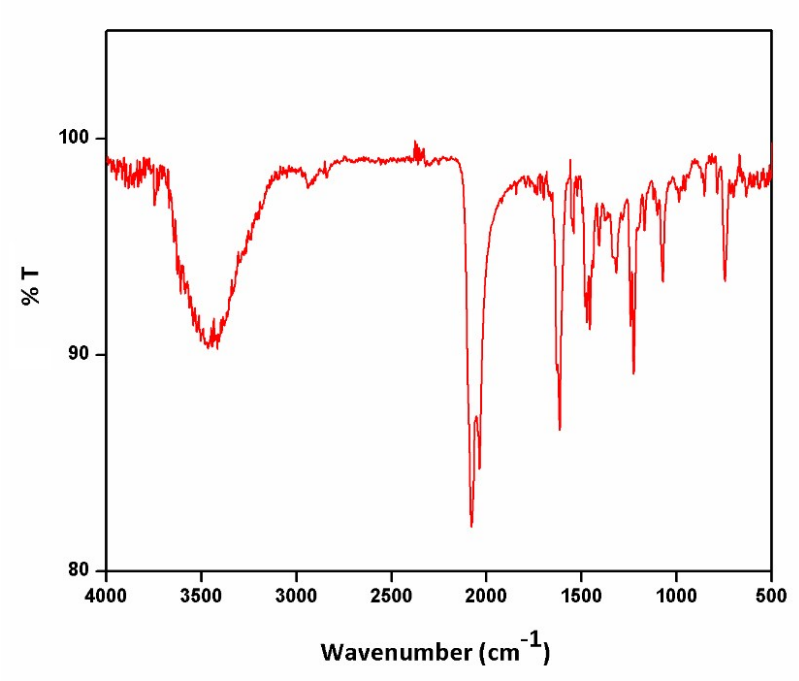

Fig. S5. Solid state (KBr pellet) IR spectrum of the complex.

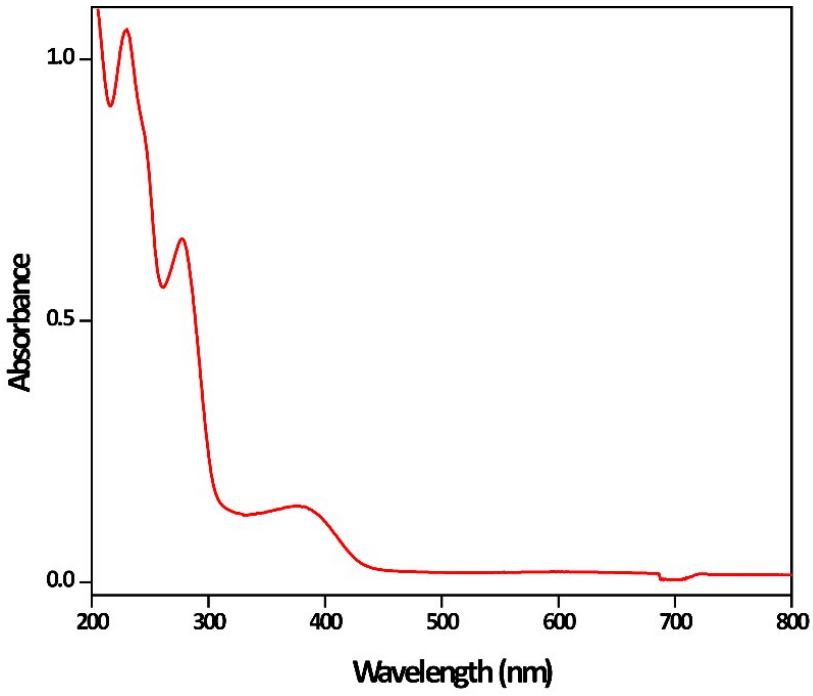

Fig. S6. Electronic spectrum of the complex in DMSO.

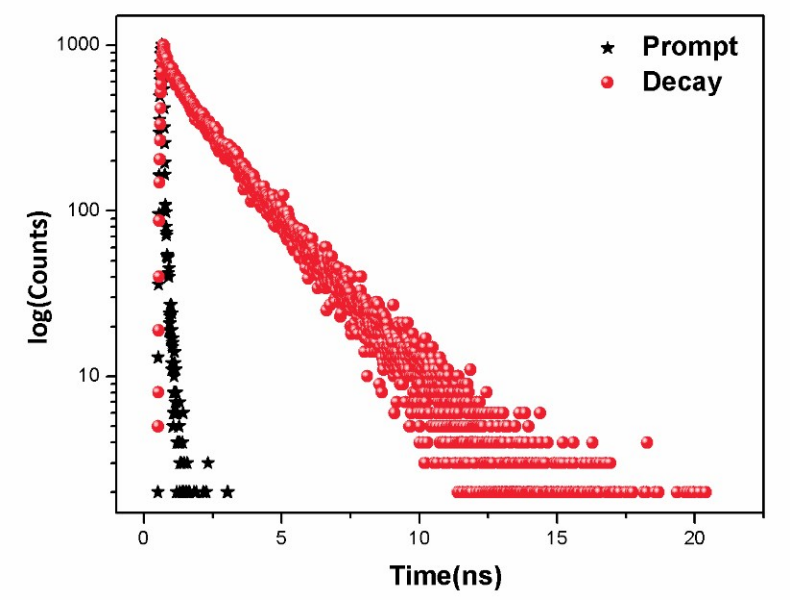

Fig. S7. Time dependent photoluminescence decay profile of the complex in DMSO.

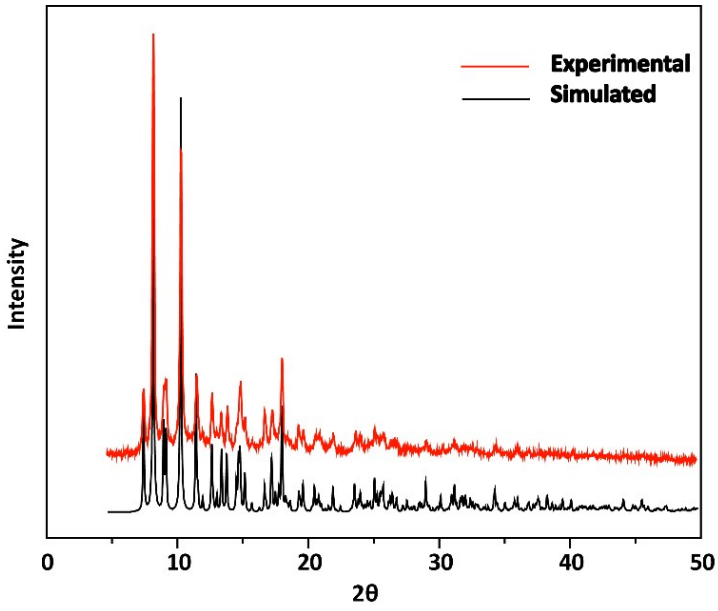

Fig. S8. Experimental and simulated PXRD patterns of the complex confirming the purity of bulk material.

Table S1: Selected bond lengths (Å) around nickel(II) for the complex.

Ni(1)-*O*(1)	2.014(2)	Ni(3)-*O*(6)	2.034(2)
Ni(1)-*O*(3)	2.286(3)	Ni(3)-*O*(10)	2.104(3)
Ni(1)-*O*(4)	2.028(2)	Ni(3) – N(10)	2.141(4)
Ni(1) – N(1)	2.168(3)	Ni(3) – N(11)	2.151(4)
Ni(1) – N(2)	2.027(3)	Ni(3) – N(12)	2.060(3)
Ni(1) – N(5)	2.098(3)	Ni(3) – N(15)	2.179(3)
Ni(2)-*O*(4)	2.040(2)	Ni(4) - *O*(6)	2.040(2)
Ni(2)-*O*(5)	2.107(3)	Ni(4) - *O*(7)	2.297(3)
Ni(2) – N(3)	2.172(4)	Ni(4) - *O*(8)	2.013(2)
Ni(2) – N(4)	2.048(3)	Ni(4) – N(13)	2.160(3)
Ni(2) – N(5)	2.164(3)	Ni(4) – N(14)	2.020(3)
Ni(2) – N(8)	2.135(3)	Ni(4) – N(15)	2.081(4)

Table S2: Selected bond angles (°) around nickel(II) for the complex.

O(1) – Ni(1) – *O*(3)	82.23(10)	*O*(6) – Ni(3) – *O*(10)	88.88(11)
O(1) – Ni(1) – *O*(4)	87.06(10)	*O*(6) – Ni(3) – N(10)	89.87(12)
O(1) – Ni(1) - N(1)	172.86(12)	*O*(6) – Ni(3) – N(11)	173.70(13)
O(1) – Ni(1) - N(2)	87.02(11)	*O*(6) – Ni(3) – N(12)	88.46(11)
O(1) – Ni(1) - N(5)	89.17(11)	*O*(6) – Ni(3) – N(15)	79.00(11)
O(3) – Ni(1) – *O*(4)	74.99(10)	*O*(10) – Ni(3) – N(10)	177.74(14)
O(3) – Ni(1) - N(1)	91.34(11)	*O*(10) – Ni(3) – N(11)	92.36(14)
O(3) – Ni(1) - N(2)	101.44(12)	*O*(10) – Ni(3) – N(12)	88.16(12)

O(3) – Ni(1) - N(5)	154.57(11)	*O*(10) – Ni(3) – N(15)	87.65(12)
O(4) – Ni(1) - N(1)	94.29(10)	N(10) – Ni(3) - N(11)	89.09(15)
O(4) – Ni(1) - N(2)	173.46(10)	N(10) – Ni(3) - N(12)	89.92(13)
O(4) – Ni(1) - N(5)	80.74(10)	N(10) – Ni(3) - N(15)	93.96(13)
N(1) – Ni(1) - N(2)	91.24(12)	N(11) – Ni(3) - N(12)	97.75(14)
N(1) – Ni(1) - N(5)	97.97(12)	N(11) – Ni(3) - N(15)	94.88(14)
N(2) – Ni(1) - N(5)	101.96(12)	N(12) – Ni(3) - N(15)	166.85(14)
O(4) – Ni(2) – *O*(5)	87.46(12)	*O*(6) – Ni(4) - *O*(7)	74.17(9)
O(4) – Ni(2) - N(3)	173.56(12)	*O*(6) – Ni(4) - *O*(8)	86.52(10)
O(4) – Ni(2) - N(4)	88.88(12)	*O*(6) – Ni(4) - N(13)	95.22(11)
O(4) – Ni(2) – N(5)	78.90(11)	*O*(6) – Ni(4) - N(14)	170.54(12)
O(4) – Ni(2) - N(8)	91.69(14)	*O*(6) – Ni(4) - N(15)	81.19(11)
O(5) – Ni(2) - N(3)	92.19(12)	*O*(7) – Ni(4) - *O*(8)	83.30(10)
O(5) – Ni(2) - N(4)	88.19(12)	*O*(7) – Ni(4) - N(13)	91.55(11)
O(5) – Ni(2) - N(5)	88.31(12)	*O*(7) – Ni(4) - N(14)	98.78(12)
O(5) – Ni(2) - N(8)	177.75(13)	*O*(7) – Ni(4) - N(15)	154.41(10)
N(3) – Ni(2) - N(4)	97.54(14)	*O*(8) – Ni(4) - N(13)	173.92(12)
N(3) – Ni(2) - N(5)	94.67(13)	*O*(8) – Ni(4) - N(14)	86.38(11)
N(3) – Ni(2) - N(8)	88.89(14)	*O*(8) – Ni(4) - N(15)	88.48(11)
N(4) – Ni(2) - N(5)	167.43(13)	N(13) – Ni(4) - N(14)	91.22(12)
N(4) – Ni(2) - N(8)	89.70(13)	N(13) – Ni(4) - N(15)	97.54(12)
N(5) – Ni(2) - N(8)	93.58(13)	N(14) – Ni(4) - N(15)	104.86(13)

Table S3: Hydrogen bond lengths [Å] and angles [°].

D–H•••A	D–H (Å)	D•••A (Å)	H•••A (Å)	∠D–H•••A (°)
O(5)-H(5C)•••O(12)	0.80	2.975	2.19	164
O(5)-H(5D)•••O(1)	0.76	2.593	1.85	166
O(10)-H(10A)•••O(14)^{i}	0.91	3.022	2.17	157
O(10)-H(10B)•••O(8)	0.72	2.610	1.95	153

Symmetry Transformation: ^{i} = -1+x,y,-1+z. D = donor; H = hydrogen; A = acceptor.

Table S4: Geometric features (distances in Å and angles in °) of the C–H···π interactions.

C–H···Cg(Ring)	H···Cg (Å)	C–H···Cg (°)	C···Cg (Å)
C(1)–H(1A)···Cg(16)^{ii}	2.80	129	3.484(5)
C(2)–H(2C)···Cg(15)	2.75	150	3.612(5)
C(39)–H(39B)···Cg(16)	3.00	129	3.678(5)
C(40)–H(40A)···Cg(13)^{iii}	2.97	130	3.664(7)
C(41)–H(41B)···Cg(14)	2.69	149	3.549(5)

Symmetry Transformations: ^{ii} = -x,1/2+y,1-z; ^{iii} = 1-x,-1/2+y,2-z.

Cg(13) = Centre of gravity of the ring **R^{13}** [C(7)–C(8)–C(9)–C(10)–C(11)–C(12)]; Cg(14) = Centre of gravity of the ring **R^{14}** [C(20)–C(21)–C(22)–C(23)–C(24)–C(25)]; Cg(15) = Centre of gravity of the ring **R^{15}** [C(33)–C(34)–C(35)–C(36)–C(37)–C(38)] and Cg(16) = Centre of gravity of the ring **R^{16}** [C(46)–C(47)–C(48)–C(49)–C(50)–C(51)] for the complex.